



TECHNISCHE UNIVERSITÄT BERLIN

On the homogenization of microstructured surfaces

Adrien Semin Kersten Schmidt

Preprint 2016/13

Preprint-Reihe des Instituts für Mathematik
Technische Universität Berlin
Preprint 2016/13

ON THE HOMOGENIZATION OF MICROSTRUCTURED SURFACES

ADRIEN SEMIN

*Institut für Mathematik, Technische Universität Berlin,
Sekretariat MA 6-4, Straße des 17. Juni 136,
Berlin, 10555, Germany
adrien.semin@math.tu-berlin.de*

KERSTEN SCHMIDT

*Institut für Mathematik, Technische Universität Berlin,
Sekretariat MA 6-4, Straße des 17. Juni 136,
Berlin, 10555, Germany
kersten.schmidt@math.tu-berlin.de*

The present work deals with the resolution of an elliptic partial differential equation in a bounded domain made of a thin and periodic layer of finite length. We provide a method to derive an efficient macroscopic representation of the solution which takes into account the boundary layer effect occurring in the vicinity of the periodic layer as well as the corner singularities appearing in the neighborhood of the extremities of the layer. Our approach combines the method of matched asymptotic expansions and the method of surface homogenization. This method is shown with the example of the Helmholtz equation.

Keywords: Asymptotic analysis; periodic surface homogenization; singular asymptotic expansions; stress intensity factor; numerical methods.

AMS Subject Classification: 32S05, 35C20, 35J05, 35J20, 41A60, 65D15

Introduction

Surfaces with a microstructures show effective properties like an absorption of acoustic waves or an impedance for electric fields where much less needs of material or volume of air is needed as if solutions without a microstructure are used. In many engineering applications microstructured surfaces are used to create and tailor such effective properties. Most prominently are microperforated absorbers and liners (see Fig. 1, Ref. 5 and Ref. 23) for the reduction of acoustic noise of vehicles or aircrafts or for optimal acoustics in conference or lecture halls. These plates with an array of perforations above a chamber or an array of chambers each of little volume, where

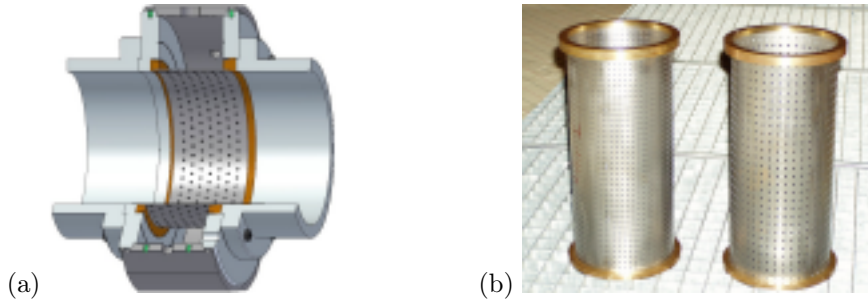


Fig. 1: Illustration of (a) the bias flow liner in an acoustic channel with circular cross-section (DUCT-C) at the institute of Institute of Propulsion Technology at DLR Berlin and (b) liners of different porosity (courtesy of F. Bake, DLR Berlin).

the size and distance of the holes are much smaller than the wavelength of the acoustic waves, lead to a damping of waves in a broad or narrow frequency range. Probably equally known is the Faraday cage where a mesh of thin conductors leads to an effective electric shielding. Various examples are shown in Fig. 2, so a channel that is connected to a side chamber by a perforated wall, a channel with a perforated wall in its cross-section and the cross-section of a channel in 3D including a circular wall where a part of is multiperforated. Direct numerical simulations are exorbitantly expensive for a high porosity as for an accurate computation, *e. g.*, with the finite element or finite difference method the size of (at least some) mesh cells or the grid size have to be at the order of the small scale or even smaller.

Even so the nature of each of these effects is different due to the different physical phenomena on the microscopic level they all can be modelled in a similar way by a homogenization procedure along the surface. Exactly as the homogenization of volumic microstructures ¹ this *surface homogenization* leads to models with effective parameters representing the microstructure, which can be resolved numerically with

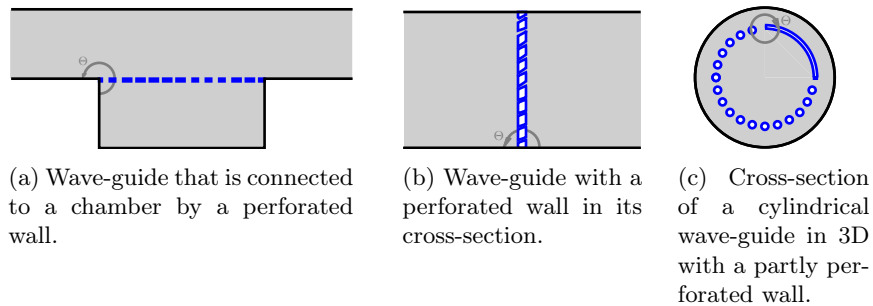


Fig. 2: Illustration of configurations of multiperforated absorbers. The end-points of the multiperforated walls meet the domain boundary at different angles Θ .

a computational effect independently of the ratio of macroscopic and microscopic scales. The procedure of the surface homogenization differs much from the original volumic one, and we expect numerical methods based on this asymptotic solution representation to differ from the numerical methods for the volumic microstructures^{4,15}. The surface homogenization leads to effective boundary or transmission conditions^{2,6,9,18,30}, which have to be corrected at the end-points points to represent the interaction of the microstructure and the singularities correctly (this has been done for the Poisson problem^{10,11} and for the Helmholtz problem¹²). Especially the interaction with the singular behaviour, that is macroscopically measurable, is mathematically involved. It is based on an extension of the singularity theory by Kondratev is needed²². This theory is due to Nazarov in 1991 in Ref. 27 who has introduced the theory for oscillating boundaries ending at a corner (see also Ref. 29 and Section 17 of Ref. 26).

In this article the surface homogenization is presented as a general methodology for an effective description and numerical modelling of microstructured surfaces incorporating the interacting with the singular behaviour at its end-points.

The outline of the paper is as follows. Section 1 is dedicated to the major ideas of the surface homogenization in presence of singularities. Based on the solution representation consisting of its macroscopic part, the boundary layer and its near field part effective transmission condition and corner conditions for the macroscopic solution at the limit interface or limit end-points of the microstructured layer, respectively, are introduced. How the nature of the transmission conditions is result of the existence properties of solutions of cell problems for one period of the microstructured layer (see Fig. 4a) and how its parameters are obtained by pre-computations of these solutions is explained in Section 2. Then, in Section 3 the relation of the singular behaviour of the macroscopic part of the solution and the near field part close to the layer end-points is explained. Finally, in Section 4 the accuracy of the surface homogenization is illustrated on numerical experiments.

1. Surface homogenization for microstructured layers with singularities

The obstacles are taken into account either through boundary conditions on its boundary or through some variation of the coefficients of the differential equation in the microstructured layer.

Let δ be the characteristic distance between two consecutive holes or two consecutive obstacles of the microstructured layer (see *e.g.* Fig. 5a). Let $D(\xi)$ be a complex $(m \times 1)$ vector linearly dependent on the variable $\xi = (\xi_1, \xi_2)$. Furthermore, let A^δ, B^δ be two functions with values in the space of complex $(m \times m)$ matrices, $(A^\delta, B^\delta) \in C^\infty(\Omega^\delta)^{m \times m}$. We assume that the matrices $A^\delta(\mathbf{x})$ and $B^\delta(\mathbf{x})$ differ of limit matrices $A^0(\mathbf{x})$ and $B^0(\mathbf{x})$ in a vicinity of the microstructured layer.

In the domain Ω^δ , we consider the general problem

$$\begin{aligned}\mathcal{L}^\delta(\mathbf{x}, \nabla_{\mathbf{x}})u &= f, & \text{in } \Omega^\delta, \\ \mathcal{N}^\delta(\mathbf{x}, \nabla_{\mathbf{x}})u &= g, & \text{on } \partial\Omega^\delta,\end{aligned}\tag{1.1}$$

where the operators \mathcal{L}^δ and \mathcal{N}^δ are defined by

$$\mathcal{L}^\delta(\mathbf{x}, \xi) = D(-\xi)A^\delta(\mathbf{x})D(\xi), \quad \mathcal{N}^\delta(\mathbf{x}, \xi) = D(\mathbf{n})B^\delta(\mathbf{x})D(\xi),\tag{1.2}$$

\mathbf{n} being the unit exterior normal vector on $\partial\Omega^\delta$. We introduce in a similar way the operators \mathcal{L}^0 and \mathcal{N}^0 associated to the matrices A^0 and B^0 . We assume moreover that problem (1.1) is well-posed for any δ and admits a solution in a variational space $\mathcal{V}^\delta(\Omega^\delta)$.

We are going to present the surface homogenization with singularities in a general setting, which we will illustrate on the following example.

Example 1.1. We consider for illustration the Helmholtz problem with homogeneous wave-number k_0 in a wave-guide that is connected to a chamber by a multiperforated wall with holes of distance δ and opening width $\eta(\delta)$. The computational domain $\Omega^\delta = \Omega \setminus \Omega_{\text{hole}}^\delta$ with the periodic array of obstacles $\Omega_{\text{hole}}^\delta \subset (-L, L) \times (-\delta, \delta)$ and the limit domain $\Omega \setminus \Gamma$ and limit interface Γ are illustrated in Figure 5. This Helmholtz problem can be stated as

$$\begin{aligned}\Delta u^\delta + k_0^2 u^\delta &= 0, & \text{in } \Omega^\delta, \\ \nabla u^\delta \cdot \mathbf{n} &= 0, & \text{on } \partial\Omega^\delta \setminus \Gamma_R, \\ \nabla(u^\delta - u_{\text{inc}}) \cdot \mathbf{n} - ik_0(u^\delta - u_{\text{inc}}) &= 0, & \text{on } \Gamma_R,\end{aligned}\tag{P}$$

where u_{inc} is an incoming wave (from left or right), which can be assumed to solve the homogeneous Helmholtz equation in an infinite wave-guide with Neumann boundary conditions. In the transparent boundary condition on $\Gamma_R = \{-L', L'\} \times (0, W)$, $L' > L$ is a first-order approximation of Robin type. As incoming wave we consider for example the plane wave $u_{\text{inc}} = \exp(ik_0(x_1 - L'))$ on the left side of Γ_R and $u_{\text{inc}} = 0$ on its right side. This example corresponds to the operators

$$D(\nabla_{\mathbf{x}}) = \begin{pmatrix} \partial_{x_1} \\ \partial_{x_2} \\ 1 \end{pmatrix}, \quad A^\delta(\mathbf{x}) = \begin{pmatrix} 1 & & \\ & 1 & \\ & & -k_0^2 \end{pmatrix} = A^0(\mathbf{x}), \quad B^\delta(\mathbf{x}) = \begin{pmatrix} 1 & & \\ & 1 & \\ & & -ik_0 \mathbb{1}_{\Gamma_R}(\mathbf{x}) \end{pmatrix} = B^0(\mathbf{x}).$$

and the source terms

$$f = 0, \quad g = \mathbb{1}_{\Gamma_R}(\mathbf{x})(\nabla u_{\text{inc}} \cdot \mathbf{n} - ik_0 u_{\text{inc}}).$$

The natural spaces associated to that problem are $\mathcal{V}^\delta(\Omega^\delta) = \mathbf{H}^1(\Omega^\delta)$ and $\mathcal{V}^0(\Omega) = \mathbf{H}^1(\Omega)$.

In most cases the solution away from the layer of obstacles and the end-points, *i. e.* the *macroscopic part* of the solution, is of practical interest. For example, in a wave-guide with part of the boundary that is multiperforated (see Fig. 5a) the

transmission coefficients are of importance, which are macroscopic quantities and, more precisely, functions of the macroscopic solution³¹. However, the macroscopic part is interacting with the solution close to the layer, which we called the *boundary layer part*, and the solution close to the end-points, known as the *near-field part* (see Fig. 3). The macroscopic solution that is defined only in some distance away from the microstructured layer can be smoothly extended, however, to the mid-line of the layer Γ (see Fig. 5b) including the end-points. On the interface Γ the extensions do not match necessarily as well as their derivatives, but satisfy (effective) transmission conditions. If the macroscopic part of the solution is extended in a smooth way to the end-points, the extension is not necessarily regular, *e. g.* it may tend to infinity at the end-points of the interface Γ ^{11,12}. A similar behaviour has been observed for the macroscopic solution for problems with oscillating boundaries with corners²⁸ or a domain with rounded corners⁸.

Solution representation To obtain an effective description of the macroscopic part up to the interface Γ and its end-points the solution is analyzed asymptotically for δ based on suitable expansions for the macroscopic part, the boundary layer part and the near field part (see again Fig. 3). More precisely:

- The macroscopic part of the solution can be written as a modification of its limit term $u_{0,0}$ by correctors $u_{n,q}$ which are weighted with powers of δ , where the power is a combination of an integer and multiples of $\frac{\pi}{\Theta}$, where Θ is the opening angle at the macroscopic corner (see Figs. 2 and. 5):

$$u^\delta(\mathbf{x}) \sim u_{0,0}(\mathbf{x}) + \sum_{(n,q) \neq \mathbf{0}} \delta^{\frac{\pi}{\Theta}n+q} u_{n,q}^\delta(\mathbf{x}). \quad (1.3)$$

The macroscopic terms $u_{n,q}^\delta$ are defined in the limit domain $\Omega \setminus \Gamma$ of Ω^δ for $\delta \rightarrow 0$ (see Fig. 5b), *i. e.*, up to the corners and the limit interface Γ , where they might be two-sided.

- The boundary layer part of the solution corrects its macroscopic part in the neighbourhood on the microstructured layer and each macroscopic term $u_{n,q}^\delta$ is corrected by a boundary layer term $\Pi_{n,q}^\delta(\mathbf{x}_\Gamma, \mathbf{X})$ depending on the nearest point \mathbf{x}_Γ of a point \mathbf{x} in this neighbourhood on the interface Γ and the scaled coordinate $\mathbf{X} = (\mathbf{x} - \mathbf{x}_\Gamma)/\delta$ (see diagonally hatched area in Fig. 3) and lead to transmission conditions (see Section 2). The boundary layer terms $\Pi_{n,q}^\delta$ are defined in canonical periodicity cells (see, *e. g.*, Fig. 4a or 4b).
- The near field part of the solution corrects its macroscopic part in the neighbourhood on the end-points of the microstructured layer and each macroscopic term $u_{n,q}^\delta$ is corrected by a near field term $U_{n,q}^\delta(\mathbf{X}^\pm)$ close to the end-point \mathbf{x}_O^\pm depending on the scaled coordinate $\mathbf{X}^\pm = (\mathbf{x} - \mathbf{x}_O^\pm)/\delta$ (see vertically hatched area in Fig. 3). The near field terms $U_{n,q}^\delta$ are defined in canonical domains of the vicinity of one end-point (see, *e. g.*, Fig. 4d or 4e) and lead to corner conditions (see Section 3).

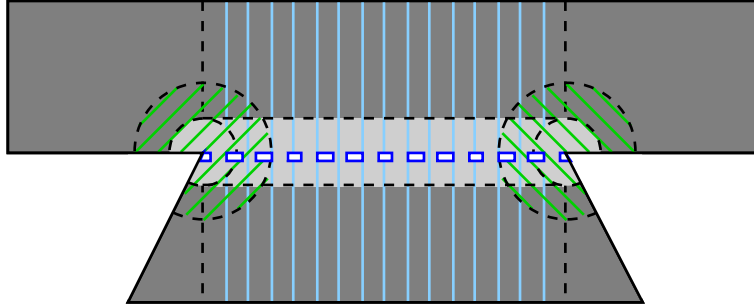


Fig. 3: Schematic representation of the overlapping subdomains for the asymptotic expansion. The macroscopic area (*dark gray*), away from the corners \mathbf{x}_O^\pm and from the limit interface Γ , the boundary layer area (*light blue vertically hatched*) and the near field areas (*light green diagonally hatched*) are overlapping each other.

Numerical computation of an effective macroscopic approximation In this paper, we show how to compute the terms of the solution representation numerically after each other. In this way an approximation to the macroscopic part of the solution is obtained that is computable with an effort that is independent of the number of obstacles or its characteristic size δ . For this some pre-computations are performed in domains, which are canonical to the boundary layer part and the near field part of the solution (see Section 2). This is first a domain (see Fig. 4a), which is obtained by taking a zoom around one obstacle, where the end-points of the layer and all the other boundaries are relegated towards infinity. The interaction with the other obstacles are taking into account by regarding a periodicity cell of the now infinite array of obstacles. Second, pre-computations are performed on a domain which is obtained by taking a zoom to the end-points of the array obstacles, where the part of boundary that is not touching the end-point, including the other end-point, is relegated to infinity (see Section 3). In this way, a conical domain with a semi-infinite array of obstacles of size and distance of order 1 as shown in Fig. 4d is obtained. This domain has still an infinite number of obstacles and we propose to approximate the near field solution on a truncated sub-domain with well-chosen boundary conditions based on its properties towards infinity.

After this pre-computations, we compute the terms of the macroscopic expansion step-by-step (see Section 4). Each term of the macroscopic expansion depends only on the previous terms. However, each corrector term of the limit solution is singular at the end-points of Γ . More precisely, they increase towards infinity when approaching the end-point. For this each macroscopic term to be computed is decomposed into a regular part and a singular part. The unbounded singular part is given analytically as a function of the previous terms, whereas the regular part lives in an usual Sobolev space like $H^1(\Omega \setminus \Gamma)$ and can be computed with classical

adaptive finite element methods³², where the data depends on the terms of lower order.

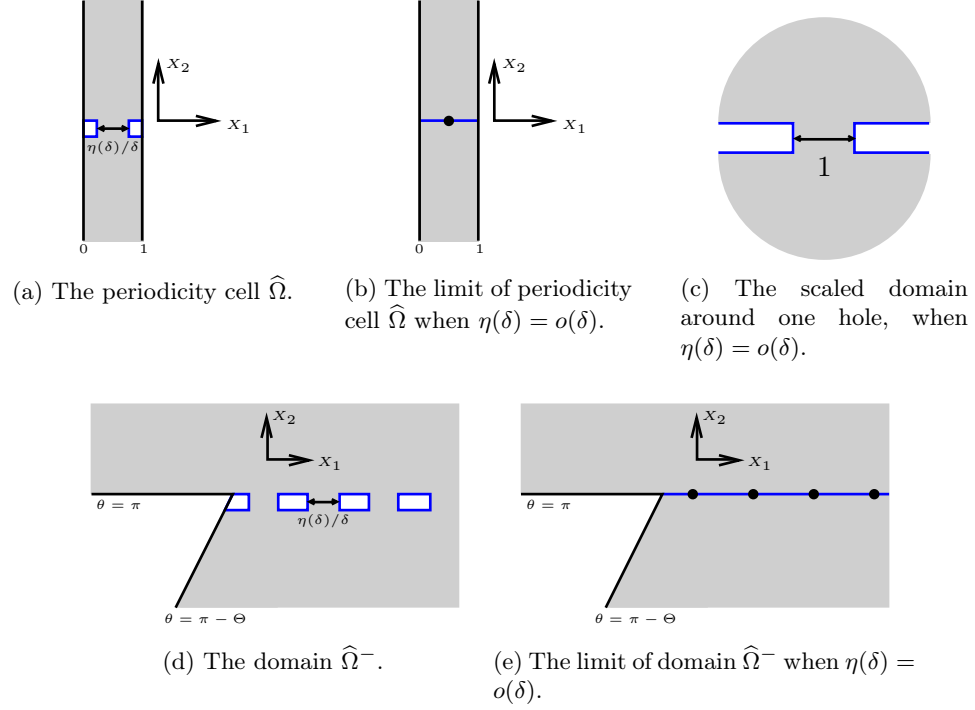


Fig. 4: The periodicity cell $\hat{\Omega}$ and the normalized domain $\hat{\Omega}^-$.

Justification with error estimates The asymptotic solution representation can be verified theoretically, which has been done in Ref. 10 for the Poisson problem in a wave-guide with Dirichlet boundary conditions connected to chamber by multi-perforated wall and in Ref. 12 for the Helmholtz problem with Neumann boundary conditions. The error estimates are based on the above mentioned theory of the solutions of the near field problems in the conical domain with the semi-infinite array of obstacles (see Fig. 4d) in special weighted Sobolev spaces and a matching procedure of the different expansions.

In general, one expects an optimal macroscopic modelling error in a subdomain Ω_α of Ω^δ of fixed distance $\alpha > 0$ away from the microstructured layer that is of the order of the first neglected term, *i. e.*, for any $s > 0$ it holds in the energy norm of the problem

$$\|u^\delta - \sum_{\substack{\pi \\ \Theta}}^{\pi} \delta^{\frac{\pi}{\Theta} n + q} u_{n,q}^\delta\|_{\Omega_\alpha} = O(\delta^s |\ln \delta|^{\kappa(s)}), \quad (1.4)$$

where $\kappa(s) \in \mathbb{N}$ depends on s . An optimal error also in the vicinity of the microstructured layer can be expected if combinations of the macroscopic terms and near field terms multiplied with well-suited cut-off functions and respective boundary layer terms are added.

Example of a wave-guide connected to chamber by multiperforated wall

Example 1.2. We consider for numerical illustration of the example 1.1 the domain $\Omega_{\text{hole}}^\delta$ as a thin plate of length 1 (*i. e.* $L = 0.5$) and width 0.075, containing $1/\delta$ holes periodically spaced. For this domain the periodic cell domain is given by Fig. 4a, and the near-field domain close to the end-point \mathbf{x}_O^- is given by Fig. 4d. We denote by ρ the porosity of the thin plate, *i. e.* the characteristic size of a hole is $\eta(\delta) = \rho\delta$. The value of the angle at the end-points is $\Theta = 3\pi/2$. The width of the chamber and of the wave-guide are both equal to $W = 0.5$. The length of the wave-guide is $L' = 2.5$ and the wave number in (P) is $k_0 = 5\pi$.

2. The periodic layer of obstacles and transmission conditions

As it was told in the introduction, one seeks for an **effective description for the macroscopic part** taking into account the interaction with the periodic layer and the corner singularities. This section focuses on the interaction with the periodic layer. For the effective description the macroscopic solution is extended to the mid-line Γ of the layer (see Fig. 5b), however, only away from end-points, where we postpone the analysis to Sec. 3. On the mid-line Γ these extensions do not match necessarily, and the macroscopic solution as well as its derivative can become discontinuous and fulfill transmission conditions which compromise the periodic layer and its impedance in an effective way.

To expose this effective behaviour of a macroscopic solution, it is expanded in powers of δ , the distance between the size of the holes. This becomes

$$u^\delta(\mathbf{x}) = u_0^\delta(\mathbf{x}) + \delta u_1^\delta(\mathbf{x}) + \delta^2 u_2^\delta(\mathbf{x}) + \dots, \quad (2.1)$$

where the dependence of the terms u_q^δ on δ is due to the end-points, which we will suspend at this moment, and to the possibly smaller scale of the geometry (*e. g.* $\eta(\delta) = o(\delta)$ in example (P)).

It has been already widely spread in the literature that the transmission conditions for the limit solution u_0^δ take then the general form

$$(\mathcal{B}_\Gamma u_0^\delta)(\mathbf{x}) = 0 \quad \text{on } \Gamma, \quad (2.2)$$

where \mathcal{B}_Γ is an operator taking the two limits of u_0^δ and its normal derivative on Γ . For our example (P), we have

$$\mathcal{B}_\Gamma v = \begin{pmatrix} [v]_\Gamma \\ [\nabla v \cdot \mathbf{n}]_\Gamma \end{pmatrix} \quad (2.3)$$

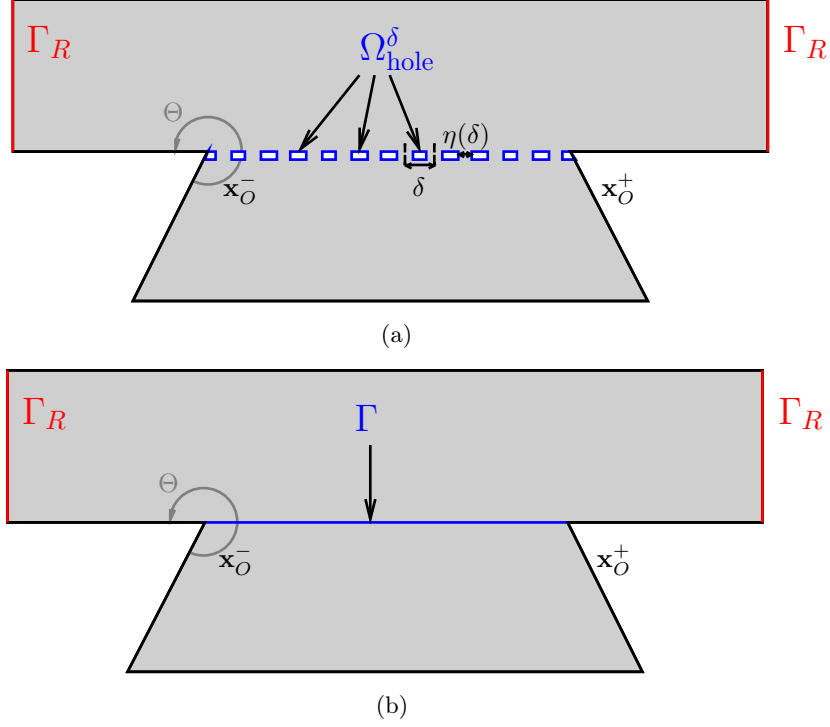


Fig. 5: Illustration of (a) the computational domain $\Omega^\delta = \overline{\Omega \setminus \Omega_{\text{hole}}^\delta}$ based on a polygonal domain Ω for Example 1.1, an acoustic wave-guide problem, and (b) its limit domain $\Omega \setminus \Gamma$ with the limit interface Γ . The microstructured layer is formed by a thin rigid wall, on which Neumann boundary conditions are posed, with an periodic array of holes of size $\eta(\delta)$ and distance δ .

for $\eta(\delta) \sim \delta$, which corresponds for the acoustics in the limit vanishing layer, and $\mathcal{B}_\Gamma v = ([v]_\Gamma - Z \langle \nabla v \cdot \mathbf{n} \rangle_\Gamma, [\nabla v \cdot \mathbf{n}]_\Gamma)^\top$ for $\delta \log \eta(\delta) \sim 1$ (i. e., $\eta(\delta) = \beta^{1/\delta}$ for some $\beta \in (0, 1)$) corresponding to an impedance boundary condition in the limit (see also Ref. 30). If Dirichlet conditions on the boundary of the obstacles of (P) are taken, then for $\eta(\delta) \sim \delta$ one obtains $\mathcal{B}_\Gamma v = ([v]_\Gamma, \langle v \rangle_\Gamma)^\top$ corresponding to a closed wall (see also Ref. 19 for the electromagnetic scattering on a cylindrical Faraday cage).

The first corrector satisfies similar transmission conditions, with a source term depending on the limit solution

$$(\mathcal{B}_\Gamma u_1^\delta)(\mathbf{x}) = (\mathcal{B}_\Gamma^1 u_0^\delta)(\mathbf{x}) \quad \text{on } \Gamma \quad (2.4)$$

as well as the higher order correctors with a source term depending on all previous

terms

$$(\mathcal{B}_\Gamma u_q^\delta)(\mathbf{x}) = \sum_{p=0}^{q-1} (\mathcal{B}_\Gamma^{q-p} u_p^\delta)(\mathbf{x}) \quad \text{on } \Gamma. \quad (2.5)$$

For our example for $\eta(\delta) \sim \delta$ we have

$$\mathcal{B}_\Gamma^1 v = \left(\begin{array}{c} 2\mathcal{D}_\infty \langle \nabla v \cdot \mathbf{n} \rangle_\Gamma \\ \mathcal{N}_0 (\partial_\Gamma^2 + k_0^2) \langle v \rangle_\Gamma \end{array} \right) \quad (2.6)$$

with two parameters $\mathcal{D}_\infty, \mathcal{N}_0 \in \mathbb{R}$.

The parameters in the transmission conditions and its nature depend on existence and uniqueness of problems with suitable boundary conditions in the periodicity cell domain $\widehat{\Omega}$ given in Fig. 4a. To defined such a domain, one has to scale around one hole with respect to δ , take an appropriate ansatz and plug this ansatz in the rescaled problem. If a smaller scale is involved (*e.g.* $\eta(\delta) = o(\delta)$), then these periodicity cell problems will contain a point contribution (see Fig. 4b), coming from resolution of another problem in a geometry scaled with $\eta(\delta)$ around one hole (see Fig. 4c)²⁴.

To obtain the parameters, in general, the solution of a cell problem has to be computed, but sometimes they appear just as a function of geometrical parameters or are even simple constants. For example, the impedance parameter Z in \mathcal{B}_Γ for the periodic wall with asymptotically small openings is a simple constant in 2D and depends on the geometry of the holes in 3D^{25,30}. In the example (P) of this article, the parameters \mathcal{D}_∞ has to be computed by such a cell problem, where $\mathcal{N}_0 = |\widehat{\Omega}_{\text{hole}}|$ is just the size of the opening in scaled coordinates.

More specifically, for this example, the condition $[u_0^\delta]_\Gamma = 0$ comes from the solution of

$$\begin{cases} -\Delta \Pi = 0, & \text{in } \widehat{\Omega}, \\ \nabla \Pi \cdot \mathbf{n} = 0, & \text{on } \partial \widehat{\Omega}_{\text{hole}} \cap \widehat{\Omega}, \end{cases} \quad (2.7)$$

where Π and its derivative are 1-periodic and Π is bounded. The boundary $\partial \widehat{\Omega}_{\text{hole}} \cap \widehat{\Omega}$ is the blue boundary on Fig. 4a. The condition $[\nabla u_0^\delta \cdot \mathbf{n}]_\Gamma$ origins from the existence of the blockage function \mathcal{D}

$$\begin{cases} -\Delta \mathcal{D} = 0, & \text{in } \widehat{\Omega}, \\ \nabla \mathcal{D} \cdot \mathbf{n} = 0, & \text{on } \partial \widehat{\Omega}_{\text{hole}} \cap \widehat{\Omega}, \end{cases} \quad (2.8)$$

where \mathcal{D} and its derivative are 1-periodic and $\mathcal{D} - X_2$ is bounded. This problems defines \mathcal{D} up to an additive constant coming from problem (2.7). This constant is set up, choosing \mathcal{D}_∞ corresponding to the limit of $\pm(\mathcal{D} - X_2)$ for $X_2 \rightarrow \pm\infty$. Then, \mathcal{N}_1 in \mathcal{B}_Γ^1 is no other than $\int_{\widehat{\Omega}} \partial_{X_1} \mathcal{D} d\mathbf{X}$.

The problem (2.8) can be solved numerically on a truncated periodicity cell $\widehat{\Omega}_B$ for given $B \geq 2$ using Dirichlet-to-Neumann (DtN) boundary operators Λ_B^\pm based on a Fourier expansion in X_1 in the spirit of Ref. 20 and Ref. 21, using

a spectral decomposition of \mathcal{D} with the theory of self-adjoint compact operators (Theorem VI.11 of Ref. 3), for $X_1 \in (0, 1)$:

$$\Lambda_B^\pm \mathcal{D}(X_1, \pm B) := - \sum_{n \neq 0} 2\pi |n| \left(\int_0^1 \mathcal{D}(\tilde{X}_1, \pm B) e^{-2i\pi n \tilde{X}_1} d\tilde{X}_1 \right) e^{2i\pi n X_1}. \quad (2.9)$$

With this DtN boundary operator, problem (2.8) can be truncated on $\widehat{\Omega}_B$, adding the condition

$$\nabla \mathcal{D} \cdot \mathbf{n} + \Lambda_B^\pm \mathcal{D} = \pm 1, \quad \text{on } \Gamma_B^\pm = (0, 1) \times \{\pm B\}, \quad (2.10)$$

and we look for a periodic solution $\mathcal{D} \in H^1(\widehat{\Omega}_B)$. We complete this problem taking the limit condition

$$\lim_{X_2 \rightarrow \pm\infty} \exp(\pi |X_2|) (\mathcal{D}(X_1, X_2) - X_2 \mp \mathcal{D}_\infty) = 0, \quad X_1 \in (0, 1). \quad (2.11)$$

into account. Using again the spectral decomposition of \mathcal{D} , we have

$$(i) \quad \int_{\Gamma_B^+} \mathcal{D} + \int_{\Gamma_B^-} \mathcal{D} = 0, \quad (ii) \quad \int_{\Gamma_B^+} \mathcal{D} - \int_{\Gamma_B^-} \mathcal{D} - 2B = 2\mathcal{D}_\infty. \quad (2.12)$$

Computations of \mathcal{D} and \mathcal{D}_∞ are illustrated for the example 1.2. The DtN operators are truncated using 8 modes (*i. e.* $-4 \leq n \leq 4$ in (2.9)).

In Fig. 6 the blockage function \mathcal{D} is plotted for different values of porosity, when the plate has four holes, *i. e.* $\delta = 1/4$ (resp. the plate has eight holes, *i. e.* $\delta = 1/8$). In Fig. 7, the blockage coefficient \mathcal{D}_∞ is plotted with respect to the characteristic size ρ of the obstacle.

3. The end-point of the periodic layer and corner conditions

In the previous section, we derived an effective description for the macroscopic part extended in the mid-line Γ , through the description of transmission conditions (2.5). The derivation of these transmission conditions is effective away from the end-points \mathbf{x}_O^\pm , then one can ask if these transmission conditions are still valid when they are to these end-points. Equivalently, one can ask himself what would be the correct singular behaviour of u_q^δ close to the end-points.

To expose this effective behaviour of a macroscopic solution, it is expanded in powers of $\delta^{\pi/\Theta}$, where Θ is the opening angle of the end-points. This becomes

$$u_q^\delta(\mathbf{x}) = u_{0,q}^\delta(\mathbf{x}) + \delta^{\pi/\Theta} u_{1,q}^\delta(\mathbf{x}) + \delta^{2\pi/\Theta} u_{2,q}^\delta(\mathbf{x}) + \dots \quad (3.1)$$

where the dependence of the terms $u_{n,q}^\delta$ on δ may be logarithmic (*i. e.* in $\ln(\delta)$) and is due to the end-point singularities, and to the possibly smaller scale (*e. g.* $\eta(\delta) = o(\delta)$ in example (P)).

For each macroscopic term $u_{n,q}^\delta$, we seek for a given stress intensity factor $s_{n,q}^\delta \notin \mathcal{V}^0(\Omega \setminus \Gamma)$, such that $u_{n,q}^\delta - s_{n,q}^\delta \in \mathcal{V}^0(\Omega \setminus \Gamma)$. Here, the set $\mathcal{V}^0(\Omega \setminus \Gamma)$ is the set of functions such that their restriction to any connected domain $K \subset \Omega$ belongs to

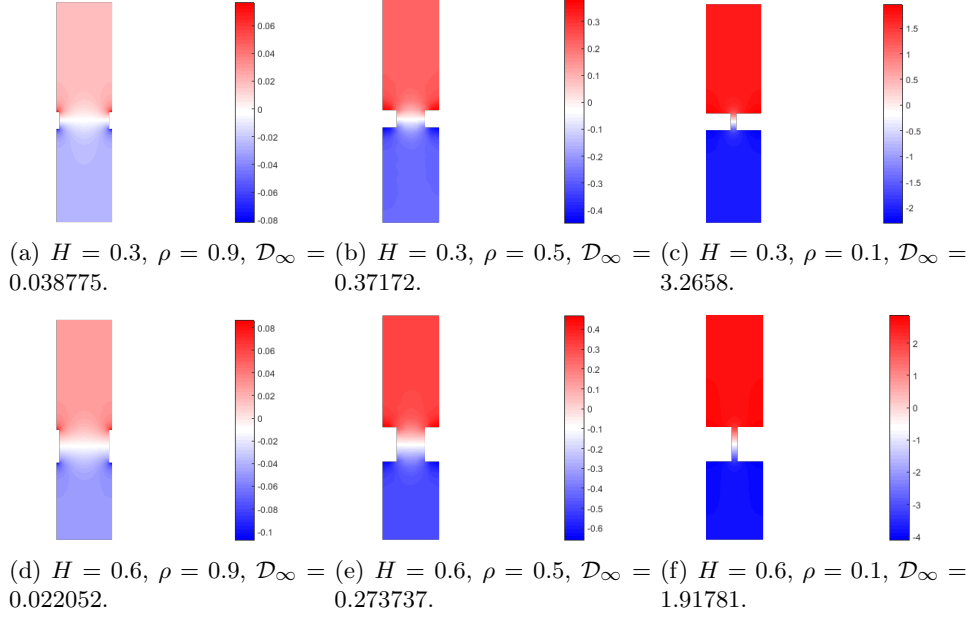


Fig. 6: Plot of $\mathcal{D} - X_2$ for different values of porosity ρ and relative wall thickness $H = 0.3$ or $H = 0.6$. The periodicity cell $\widehat{\Omega}$ is obtained by identification with $\delta = 1/4$ for $H = 0.3$ and $\delta = 1/8$ for $H = 0.6$.

$\mathcal{V}^0(K)$. Such a function has been studied *e. g.* in Ref. 13 for a domain containing a crack (*i. e.* $\Theta = 2\pi$). These stress intensity factors are separated in two cases:

- (i) due to the transmission conditions (2.4) with a source term depending on the limit solution, we obtain a singular behaviour for the first corrector close to the end-points, which is consistent with the matching with the near field. Numerical pre-computations in a neighborhood of the end-points of the periodic layer are not necessary. This point will be more deeply studied in Sec. 3.1,
- (ii) in addition higher-order correctors exhibit a singular behavior that is not caused by the source term in the transmission condition only, since this singular behavior is in the kernels of \mathcal{L}^0 and \mathcal{B}_Γ close to the end-points, but can be explained only with the matching to the near field. For this, we need pre-computations of singular enhancement functions S^\pm and singularity enhancement factors $\mathcal{L}(S^\pm)$ in a neighborhood of the end-points of the periodic layer. This point will be more deeply studied in Sec. 3.2,
- (iii) in general, a part of the singularity is correctly obtained studying the behaviour due to the source terms in the transmission conditions and a part is not correctly obtained and one needs to study the matching with the near field and pre-compute singularity enhancement functions / factors.

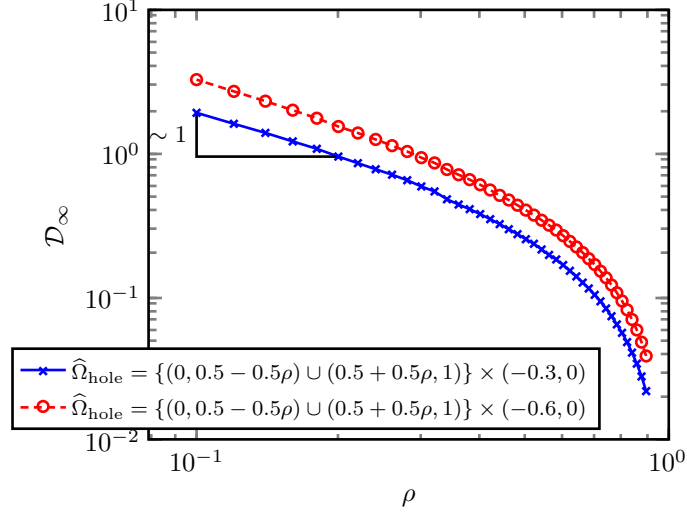


Fig. 7: Plot of \mathcal{D}_∞ with respect to the porosity ρ of the obstacle. Close to $\rho = 0$, the quantity $\mathcal{D}_\infty\rho$ remains constant.

The stress intensity factors and their nature depend on the shape of singularity enhancement functions in the two conical domains containing an infinite periodic layer $\widehat{\Omega}^\pm$ (see Fig. 4d). To define the problem whose the singular enhancement functions are solution, one has to scale around one corner with respect to δ to obtain the domain $\widehat{\Omega}^\pm$, take an appropriate ansatz and plug this ansatz in the rescaled problem. If a smaller scale is involved (*e.g.* $\eta(\delta) = o(\delta)$), then these near field problems will contain an infinite periodic point contribution (see Fig. 4e), coming from resolution of another problem in a geometry scaled with $\eta(\delta)$ around one hole (see Fig. 4c).

To obtain these functions, in general, the solution of a near field problem has to be computed (Sec. 3.2), but sometimes they can be computed analytically, using the impedance parameters that were computed in the previous section 3.1.

3.1. Singular behaviour due to source terms in the transmission conditions

In this section, we are interested into the resolution of

$$\begin{aligned} \mathcal{L}^0 v &= 0, & \text{in } \mathcal{K}^\pm \\ \mathcal{N}^0 v &= 0, & \text{on } \partial\mathcal{K}^\pm \\ \mathcal{B}_{\Gamma^\pm} v &= f, & \text{on } \Gamma^\pm, \end{aligned} \tag{3.2}$$

where $f = \mathcal{B}_{\Gamma^\pm}^1 u$, $u \in \mathcal{V}^\pm(\mathcal{K}^\pm)$ being an homogeneous solution of (3.2). Here $\mathcal{V}^\pm(\mathcal{K}^\pm)$ is the set of functions ϕ such that the function $\phi\chi_\pm \in \mathcal{V}^0(\Omega)$, where χ_\pm is

a C^∞ truncating function compactly supported in a vicinity of \mathbf{x}_O^\pm . The operators \mathcal{B}_{Γ^\pm} and $\mathcal{B}_{\Gamma^\pm}^1$ are formally the operators \mathcal{B}_Γ and \mathcal{B}_Γ^1 written on Γ^\pm instead of Γ .

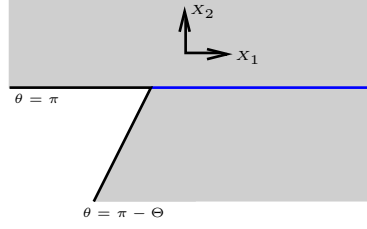


Fig. 8: Semi-infinite conical domain \mathcal{K}^- with the semi-infinite interface Γ^- (plotted in blue).

More specifically, in the example (P), close to the corner \mathbf{x}_O^\pm , the limit term $u_{0,0} \in (\mathbf{H}^1)^\pm(\mathcal{K}^\pm)$ (i. e. $u_{0,0}\chi_\pm \in \mathbf{H}^1(\Omega)$). Using again the self-adjoint operators for the 1D Laplace-Beltrami operator ∂_θ^2 with Neumann boundary conditions at $\theta^- = \{\pi - \Theta, \pi\}$ (resp. $\theta^+ = \{0, \Theta\}$), we can express $u_{0,0}$ close to the end-point \mathbf{x}_O^\pm as a linear combination of radial Bessel functions of first kind $J_{\frac{n\pi}{\Theta}}(k_0 r^\pm)$ times cosine functions in θ^\pm . Problem (3.2) with right-hand side $f := J_{\frac{n\pi}{\Theta}}(k_0 r^\pm) \cos \frac{n\pi}{\Theta}(\theta^\pm - \Theta_0^\pm)$, with $\Theta_0^- = \pi$ and $\Theta_0^+ = 0$, for $n \neq 1$, admits a solution $v \in (\mathbf{H}^1)^\pm(\mathcal{K}^\pm)$. However, the function $f := J_{\frac{\pi}{\Theta}}(k_0 r^\pm) \cos \frac{\pi}{\Theta}(\theta^\pm - \Theta_0^\pm)$ gives equivalently the condition

$$\mathcal{B}_{\Gamma^\pm} v = \begin{pmatrix} \mp 2\mathcal{D}_\infty J_{\frac{\pi}{\Theta}-1}(k_0 r^\pm) \frac{\pi}{\Theta} \sin \frac{\pi^2}{\Theta} \\ \mp \mathcal{N}_0 \frac{\pi}{\Theta} (\frac{\pi}{\Theta} - 1) J_{\frac{\pi}{\Theta}-1}(k_0 r^\pm) \cos \frac{\pi^2}{\Theta} \end{pmatrix} \quad (3.3)$$

There exists a particular solution ϕ_1^\pm of (3.2) under the form

$$\phi_1^\pm(r^\pm, \theta^\pm) = J_{\frac{\pi}{\Theta}-1}(k_0 r^\pm) \psi_1^\pm(\theta^\pm), \quad (3.4)$$

where the study of the function $\psi_1^\pm(\theta^\pm)$ is postponed in appendix Appendix A. Then, from $u_{0,0}$, we extract the contribution corresponding to the Bessel function $J_{\frac{\pi}{\Theta}}(k_0 r^\pm)$

$$\ell^\pm(u_{0,0}) = \frac{2}{\Theta J_{\frac{\pi}{\Theta}}(k_0 r^\pm)} \int_{I^\pm} u_{0,0}^\delta(r^\pm, \theta^\pm) \cos \frac{\pi}{\Theta}(\theta^\pm - \Theta_0^\pm) d\theta^\pm, \quad I^- = (\pi - \Theta, \pi), \quad I^+ = (0, \Theta), \quad (3.5)$$

then close to the corner \mathbf{x}_O^\pm , the singular behaviour of $u_{0,1}^\delta$ is given by the stress intensity factor $\frac{k_0 \Theta}{2\pi} \ell^\pm(u_{0,0}) \phi_1^\pm(r^\pm, \theta^\pm)$, i. e.

$$u_{0,1}^\delta - \sum_{\pm} \frac{k_0 \Theta}{2\pi} \ell^\pm(u_{0,0}) \phi_1^\pm \chi_\pm \in \mathbf{H}^1(\Omega_T \cup \Omega_B). \quad (3.6)$$

This last relation means that the restriction of this function to Ω_T (resp. Ω_B) is in $\mathbf{H}^1(\Omega_T)$ (resp. $\mathbf{H}^1(\Omega_B)$).

3.2. Singular behaviour coming from the matching with the near field

As it was already stated in the introduction of this section, there exists two singularity enhancement factors $\mathcal{L}(S^\pm)$ such that the singular behaviour of $u_{2,0}^\delta$ is given by the stress intensity factor

$$\begin{aligned}
 & -\pi \mathcal{L}(S^\pm) \ell^\pm(u_{0,0}) \frac{(k_0/2)^{2\pi/\Theta}}{\Gamma(\pi/\Theta)\Gamma(\pi/\Theta+1)} Y_{\frac{\pi}{\Theta}}(k_0 r^\pm) \cos \frac{\pi}{\Theta}(\theta^\pm - \Theta_0^\pm), \quad i. e. \\
 & u_{2,0}^\delta + \sum_{\pm} \pi \mathcal{L}(S^\pm) \ell^\pm(u_{0,0}) \frac{(k_0/2)^{2\pi/\Theta}}{\Gamma(\pi/\Theta)\Gamma(\pi/\Theta+1)} Y_{\frac{\pi}{\Theta}}(k_0 r^\pm) \cos \frac{\pi}{\Theta}(\theta^\pm - \Theta_0^\pm) \chi_{\pm} \in H^1(\Omega).
 \end{aligned} \tag{3.7}$$

Note that the function $\phi_2^\pm(r^\pm, \theta^\pm) := (r^\pm, \theta^\pm) \mapsto Y_{\frac{\pi}{\Theta}}(k_0 r^\pm) \cos \frac{\pi}{\Theta}(\theta^\pm - \Theta_0^\pm)$ is an homogeneous solution of (3.2).

More generally, a higher order macroscopic term has a singular behaviour as a linear combination of canonical stress intensity factors $y_{k,\pm}(r^\pm) \phi_{k,\pm}(\theta^\pm)$ solutions of (3.2) with factors that are productions of a functional of lower order macroscopic terms and a related singularity enhancement factor.

These functionals of lower order macroscopic terms are obtained projecting these terms on their regular part. For example, $\ell^\pm(u_{0,0})$ is given by relation (3.5).

To obtain the singular enhancement factor $\mathcal{L}(S^\pm)$, one has to compute a particular near field function (also called singular enhancement function) S^\pm in a stretched multi-perforated domain around one end-point (see Fig. 4d) solution of a Laplace equation with a prescribed behavior at infinity away from the perforations, *i. e.* for radial coordinate $R \rightarrow \infty$ and for θ not being the angle of the interface. More precisely, we are looking for S^\pm solution of the system

$$\begin{aligned}
 \Delta S^\pm &= 0, \quad \text{in } \widehat{\Omega}^\pm, \\
 \nabla S^\pm \cdot \mathbf{n} &= 0, \quad \text{on } \partial \widehat{\Omega}^\pm, \\
 S^\pm - R^{\pi/\Theta} \cos \frac{\pi}{\Theta}(\theta^\pm - \Theta_0^\pm) &= o(1), \quad R \rightarrow \infty, \theta \neq \pi - \Theta_0^\pm
 \end{aligned} \tag{3.8}$$

We can see that the equation and the boundary conditions we have to consider are no other than the principal symbol of the Helmholtz equation and the Neumann boundary condition of (P). In the general case linear operators $\mathcal{L}^0, \mathcal{N}^0$ given *e. g.* by (3.2), denoting respectively L^0, N^0 their principal part, we have to solve

$$\begin{aligned}
 L^0 V &= F, \quad \text{in } \widehat{\Omega}^\pm, \\
 N^0 V &= G, \quad \text{on } \partial \widehat{\Omega}^\pm,
 \end{aligned} \tag{3.9}$$

with a prescribed behavior towards infinity coming from the expansion of the homogeneous solutions of (3.2). Such a problem has been studied by Sergei Nazarov in the case of a periodic boundary with Dirichlet boundary conditions²⁷ and with Neumann boundary conditions²⁹ for a general linear differential operator and has been studied by the authors^{10,12} and relies on the use of Mellin transform, as well as on the extension of the Kondrat'ev theory²². The possible right hand-sides F and G in (3.9) would come from the study of the high-order near field terms.

The standard variational space to solve problem (3.9) in the case of the Laplace equation is

$$\mathcal{V}^\pm(\widehat{\Omega}^\pm) = \left\{ V \in \mathbf{H}_{\text{loc}}^1(\widehat{\Omega}^\pm), \nabla V \in \mathbf{L}^2(\widehat{\Omega}^\pm), \frac{V}{(1+R)\ln(2+R)} \in \mathbf{L}^2(\widehat{\Omega}^\pm) \right\}, \quad (3.10)$$

which, equipped with the norm

$$\|V\|_{\mathcal{V}^\pm(\widehat{\Omega}^\pm)}^2 = \left\| \frac{V}{(1+R)\ln(2+R)} \right\|_{\mathbf{L}^2(\widehat{\Omega}^\pm)}^2 + \|\nabla V\|_{\mathbf{L}^2(\widehat{\Omega}^\pm)}^2, \quad (3.11)$$

is a Hilbert space. However, it is clear that with the requested condition towards infinity (3.8-iii), the singular enhancement function S^\pm cannot belong to $\mathcal{V}^\pm(\widehat{\Omega}^\pm)$. Therefore, we shall decompose it into a particular function (also called asymptotic block) \mathcal{S}^\pm that has this prescribed behavior towards infinity, and its remainder $\mathcal{R}^\pm = S^\pm - \mathcal{S}^\pm$ belongs to $\mathcal{V}^\pm(\widehat{\Omega}^\pm)$. To write the asymptotic block \mathcal{S}^\pm , one starts from the limit behavior $R^{\pi/\Theta} \cos \frac{\pi}{\Theta}(\theta^\pm - \Theta_0^\pm)$. To take into account the presence of the infinite periodic layer, we multiply this limit behaviour by a smooth cut-off function $\chi(X_2)$ such that

$$\chi(t) = 0, \quad |t| < 1, \quad \chi(t) = 1, \quad |t| > 2, \quad (3.12)$$

and we go back and forth between the radial behavior of \mathcal{S}^\pm and its behavior close to the infinite periodic layer, similarly as going back and forth between the macroscopic part of the solution and its periodic layer corrector in Section 2. Therefore, the radial part of the asymptotic block \mathcal{S}^\pm can be written towards infinity as

$$\mathcal{S}^\pm = R^{\pi/\Theta} \cos \frac{\pi}{\Theta}(\theta^\pm - \Theta_0^\pm) + R^{\pi/\Theta-1} \psi_1(\theta^\pm) + O(R^{\pi/\Theta-2}), \quad (3.13)$$

the function ψ_1 in (3.13) being the same as the function defined in (3.4). In the particular case $\Theta = \pi$ (see *e.g.* 2a), we need to take into account one additional term in that expansion. Neglecting the $O(R^{\pi/\Theta-2})$ part and multiplying by $\chi(R)$ to have a regular behavior towards $R = 0$, the remainder \mathcal{R}^\pm satisfies problem (3.9) with $F = -\mathbf{L}^0 \mathcal{S}^\pm = -\Delta \mathcal{S}^\pm$ and $G = -\mathbf{N}^0 \mathcal{S}^\pm = -\nabla \mathcal{S}^\pm \cdot \mathbf{n}$. This problem is well-posed and admits a unique solution in $\mathcal{V}^\pm(\widehat{\Omega}^\pm)$. It can be shown then that the leading part of this remainder towards infinity is the same as the leading part of the problem (3.9) written on the conical domain \mathcal{K}^\pm instead on the domain $\widehat{\Omega}^\pm$, *i.e.* there exists a constant $\mathcal{L}(S^\pm)$ independent on the choice of the truncating function such that

$$\mathcal{R}^\pm \sim \mathcal{L}(S^\pm) R^{-\pi/\Theta} \cos \frac{\pi}{\Theta}(\theta^\pm - \Theta_0^\pm). \quad (3.14)$$

The problem (3.9) can be solved numerically on a truncated near field domain $\widehat{\Omega}_{R_e}^\pm$ for given $R_e \geq 2$ using an approximate Robin boundary condition using the behavior of \mathcal{R}^\pm given by (3.14). With this approximate Robin boundary condition, problem (3.9) can be truncated on $\widehat{\Omega}_{R_e}^\pm$, adding the condition

$$\nabla \mathcal{R}^\pm \cdot \mathbf{n} + \frac{\pi}{\Theta R_e} \mathcal{R}^\pm = 0, \quad \text{on } \Gamma_{R_e}^\pm, \quad (3.15)$$

where the artificial boundary $\Gamma_{R_e}^-$ is given by $\Gamma_{R_e}^- = \{(R_e \cos \theta^-, R_e \sin \theta^-), \theta^- \in (\pi - \Theta, \pi)\}$ and the artificial boundary $\Gamma_{R_e}^+$ is given similarly. Additionally, for these artificial boundaries we choose R_e such that $\Gamma_{R_e}^\pm \in \widehat{\Omega}^\pm$, *i. e.* they do not intersect any hole. Using again the behavior of \mathcal{R}^\pm (3.14), we have

$$\mathcal{L}(S^\pm) \sim \frac{2}{\Theta} R_e^{\pi/\Theta} \int_{\Gamma_{R_e}^\pm} \mathcal{R}^\pm. \quad (3.16)$$

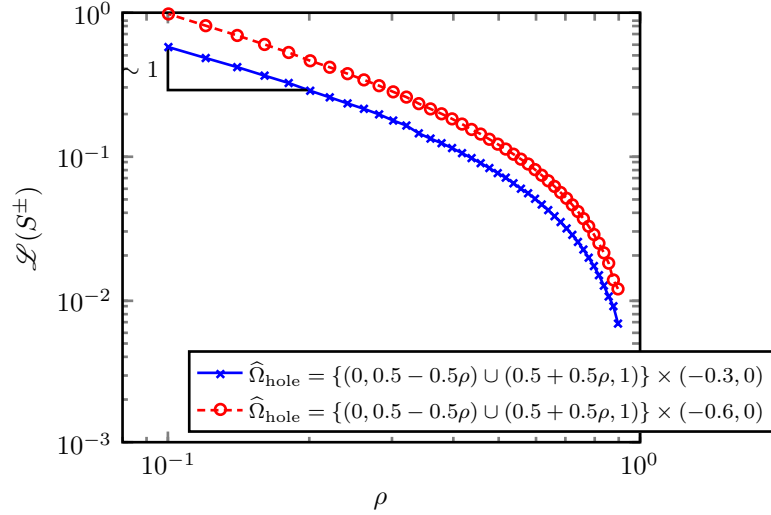


Fig. 9: Plot of $\mathcal{L}(S^\pm)$ with respect to the porosity ρ of the obstacle, for the truncating radius $R_e = 30.5$. The periodicity cell is obtained by identification with $\delta = 1/4$ for $H = 0.3$ and $\delta = 1/8$ for $H = 0.6$. Close to $\rho = 0$, the quantity $\mathcal{L}(S^\pm)\rho$ remains constant.

Computations of $\mathcal{L}(S^\pm)$ are illustrated for the example 1.2. In Fig. 9, the singular enhancement coefficient $\mathcal{L}(S^\pm)$ is plotted with respect to the characteristic size ρ of the obstacle for the truncating radius $R_e = 30.5$. In Fig. 10a, the singular enhancement coefficient $\mathcal{L}(S^\pm)$ is plotted with respect to the characteristic truncating radius R_e of the near-field domain for the porosity $\rho = 0.3$. Contrarily to the computation of the blockage coefficient \mathcal{D}_∞ which exponentially converges with respect to the characteristic domain size B (see *e. g.* Ref. 17), the convergence rate of the singular enhancement coefficient $\mathcal{L}(S^\pm)$ is only polynomial (see Fig. 10b), and at least two different computations have to be achieved (*e. g.* for $R_e = 30.5$ and $R_e = 35.5$) to obtain a good approximation of this coefficient.

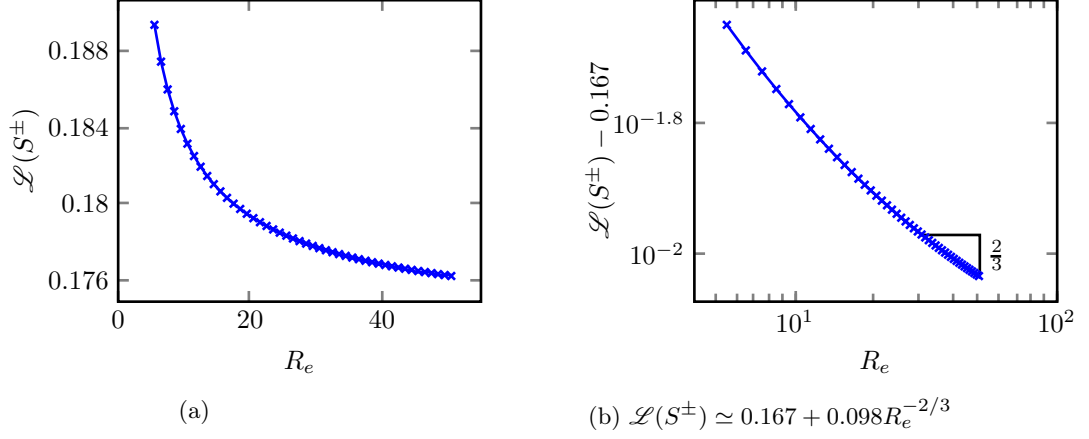


Fig. 10: Plot of $\mathcal{L}(S^\pm)$ with respect to the truncating radius R_e , for the porosity $\rho = 0.3$. The periodicity cell is obtained by identification with $\delta = 1/8$ for $H = 0.6$.

4. Computation of the macroscopic solution

This section is dedicated to the computation of each macroscopic term $u_{n,q}$ of the expansion (1.3). These terms solve the problem

$$\begin{aligned} \mathcal{L}^0(\mathbf{x}, \nabla_{\mathbf{x}})u_{n,q}^\delta &= f_{n,q}, & \text{in } \Omega \setminus \Gamma, \\ \mathcal{N}^0(\mathbf{x}, \nabla_{\mathbf{x}})u_{n,q}^\delta &= g_{n,q}, & \text{on } \partial\Omega, \end{aligned} \quad (4.1)$$

with the transmission condition given by (2.5)

$$(\mathcal{B}_\Gamma u_{n,q}^\delta)(\mathbf{x}) = \sum_{p=0}^{q-1} (\mathcal{B}_\Gamma^{q-p} u_{n,p}^\delta)(\mathbf{x}) \quad \text{on } \Gamma. \quad (4.2)$$

and with possibly corner singularities that have been studied in Section 3. One important point to notice that, as it was already explained in Section 1, the computational effort of each macroscopic term is independent of the parameter δ , since the linear differential operators involved in these equations, as well as the computational domain, are independent of δ .

In the following, the different macroscopic terms of the expansion are computed for the example (P) (Section 4.1) and a finite sum of the expansion is compared with a reference solution computed by resolving all the obstacles (Section 4.2).

4.1. Computation of the macroscopic term of the expansion

For the example problem (P), the macroscopic term $u_{1,0}^\delta$ corresponding to the weight $\delta^{\pi/\Theta}$ is solution of (4.1)-(4.2) with right-hand side $f_{0,0}^\delta = g_{0,0}^\delta = 0$ and contains no stress intensity factor (*i.e.* $u_{1,0}^\delta \in H^1(\Omega_T \cup \Omega_B)$). Then it stands $u_{1,0}^\delta = 0$. In a similar way, and using the transmission conditions (4.2), the macroscopic term $u_{1,1}^\delta$

corresponding to the weight $\delta^{\pi/\Theta+1}$ is equal to 0. Therefore the first non-negligible macroscopic terms are $u_{0,0}^\delta$, $u_{0,1}^\delta$ and $u_{2,0}^\delta$.

Numerical simulations are carried using the C++ Finite Elements Library Concepts^{7,14}. These terms are computed on a mesh generated using GMSH¹⁶. This mesh is refined close to the corners and solves the limit interface Γ (see Fig. 11). In particular, the interface Γ is refined close to the end-points.

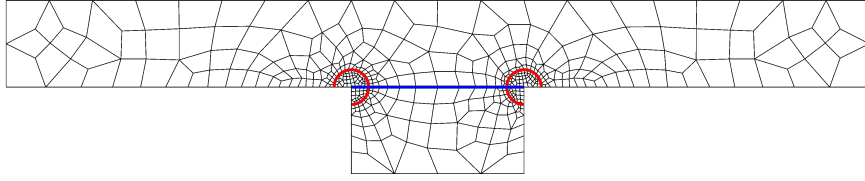


Fig. 11: Mesh used for the computation of the macroscopic solution. The blue line is the limit interface Γ . The red arcs are the domain integration to get the functionals $\ell^\pm(u_{0,0})$. These lines are resolved by this mesh.

Computation of the limit solution In this paragraph, the problem (4.1)-(4.2) for $n = q = 0$, with $f_{0,0} = 0$ and $g_{0,0} = \mathbb{1}_{\Gamma_R}(\nabla u_{\text{inc}} \cdot \mathbf{n} - ik_0 u_{\text{inc}})$ is studied. The transmission condition (4.2) gives nothing other than no jump conditions, so that the limit interface Γ is transparent for $u_{0,0}^\delta$. This problem admits then a unique solution $u_{0,0} \in H^1(\Omega)$ independent of δ and is resolved numerically using an hp -refinement strategy towards the end-points.

From the resolution of this limit problem, we compute the trace operator $\mathcal{B}_\Gamma^1 u_{0,0}$ on Γ using (2.6) and the values $\ell^\pm(u_{0,0})$ that will be used for the determination of the stress intensity factors of the upcoming terms.

Computation of the corrector $u_{0,1}^\delta$ In this paragraph, the problem (4.1)-(4.2) for $n = 0, q = 1$, with $f_{0,1} = g_{0,1} = 0$ and with the transmission operator \mathcal{B}_Γ^1 given by (2.6)

$$\mathcal{B}_\Gamma^1 v = \begin{pmatrix} 2\mathcal{D}_\infty \langle \nabla v \cdot \mathbf{n} \rangle_\Gamma \\ \mathcal{N}_0(\partial_\Gamma^2 + k_0^2) \langle v \rangle_\Gamma \end{pmatrix}$$

is studied. Moreover, $u_{0,1}^\delta$ admits a prescribed stress intensity factor given by the relation (3.6)

$$u_{0,1}^\delta - \sum_{\pm} \frac{k_0 \Theta}{2\pi} \ell^\pm(u_{0,0}) \phi_\Gamma^\pm \chi_\pm \in H^1(\Omega_T \cup \Omega_B).$$

To solve this problem, one has to introduce the function $\tilde{u}_{0,1}^\delta \in H^1(\Omega_T \cup \Omega_B)$ corresponding to the regular part of $u_{0,1}^\delta$, by subtracting its stress intensity factor

from itself. Therefore, the function $\tilde{u}_{0,1}^\delta$ has to satisfy the following problem

$$\begin{aligned} \mathcal{L}^0(\mathbf{x}, \nabla_{\mathbf{x}})\tilde{u}_{0,1}^\delta &= - \sum_{\pm} \frac{k_0\Theta}{2\pi} \ell^\pm(u_{0,0}) \mathcal{L}^0(\mathbf{x}, \nabla_{\mathbf{x}})(\phi_1^\pm \chi_\pm), & \text{in } \Omega \setminus \Gamma, \\ \mathcal{N}^0(\mathbf{x}, \nabla_{\mathbf{x}})\tilde{u}_{0,1}^\delta &= - \sum_{\pm} \frac{k_0\Theta}{2\pi} \ell^\pm(u_{0,0}) \mathcal{N}^0(\mathbf{x}, \nabla_{\mathbf{x}})(\phi_1^\pm \chi_\pm), & \text{on } \partial\Omega, \\ (\mathcal{B}_\Gamma \tilde{u}_{0,1}^\delta)(\mathbf{x}) &= (\mathcal{B}_\Gamma^1 u_{0,0}^\delta)(\mathbf{x}) - \sum_{\pm} \frac{k_0\Theta}{2\pi} \ell^\pm(u_{0,0}) (\mathcal{B}_\Gamma \phi_1^\pm \chi_\pm)(\mathbf{x}), & \text{on } \Gamma. \end{aligned} \quad (4.3)$$

Problem (4.3) seems *a priori* as complicated to solve as the problem satisfied by $u_{0,1}^\delta$, since the right-hand side of the first line, for example, could not possibly belong to $L^2(\Omega)$. Hopefully, since the singular enhancement function ϕ_1^\pm is solution of (3.2), a suitable choice for the cut-off functions χ_\pm would be cut-off functions that are identically equal to 1 in a vicinity of the end-points \mathbf{x}_O^\pm . To do so, being two suitable numbers $r_i < r_e$, the functions χ_\pm depend only on the radius $r^\pm = |\mathbf{x} - \mathbf{x}_O^\pm|$ and is chosen such that $\chi_\pm = 1$ for $r^\pm < r_i$ and $\chi_\pm = 0$ for $r^\pm > r_e$. It will ensure then that the boundary operator $\mathcal{N}^0(\mathbf{x}, \nabla_{\mathbf{x}})$ can commute with the truncating function, *i. e.* $\mathcal{N}^0(\mathbf{x}, \nabla_{\mathbf{x}})(\phi_1^\pm \chi_\pm) = \chi_\pm \mathcal{N}^0(\mathbf{x}, \nabla_{\mathbf{x}})(\phi_1^\pm) = 0$. Introducing for a linear operator \mathcal{A} the commutator operator $[\mathcal{A}, \chi_\pm] = \mathcal{A}\chi_\pm - \chi_\pm\mathcal{A}$ which will be compactly supported in the support of $\nabla\chi_\pm$, and using that ϕ_1^\pm is solution of (3.2), problem (4.3) can be simplified to

$$\begin{aligned} \mathcal{L}^0(\mathbf{x}, \nabla_{\mathbf{x}})\tilde{u}_{0,1}^\delta &= - \sum_{\pm} \frac{k_0\Theta}{2\pi} \ell^\pm(u_{0,0}) [\mathcal{L}^0(\mathbf{x}, \nabla_{\mathbf{x}}), \chi_\pm] \phi_1^\pm, & \text{in } \Omega \setminus \Gamma, \\ \mathcal{N}^0(\mathbf{x}, \nabla_{\mathbf{x}})\tilde{u}_{0,1}^\delta &= 0, & \text{on } \partial\Omega, \\ (\mathcal{B}_\Gamma \tilde{u}_{0,1}^\delta)(\mathbf{x}) &= (\mathcal{B}_\Gamma^1 u_{0,0}^\delta)(\mathbf{x}) - \sum_{\pm} \frac{k_0\Theta}{2\pi} \ell^\pm(u_{0,0}) (\mathcal{B}_\Gamma \phi_1^\pm \chi_\pm)(\mathbf{x}), & \text{on } \Gamma. \end{aligned} \quad (4.4)$$

Numerically, the function $\tilde{u}_{0,1}^\delta$ is computed using finite elements discontinuous over the interface Γ , since the jump of $\tilde{u}_{0,1}^\delta$ across the interface Γ is non-zero. The Neumann jump of $\tilde{u}_{0,1}^\delta$ appears naturally when writing the variational formulation associated to the problem (4.4), whereas the Dirichlet jump has to be taken into account *e. g.* using a penalization method.

Computation of the corrector $u_{2,0}^\delta$ In this paragraph, as well as for the computation of the corrector $u_{0,1}^\delta$, the problem (4.1)-(4.2) for $n = 2$, $q = 0$, with $f_{2,0} = g_{2,0} = 0$, is studied. The transmission condition (4.2) gives nothing other than no jump conditions, so that the limit interface Γ is transparent for $u_{2,0}^\delta$. But, contrarily to the resolution of the limit solution, the H^1 -regularity close to the corners do not hold. Then, one has to introduce the function $\tilde{u}_{2,0}^\delta$ corresponding to the regular part of $u_{2,0}^\delta$, by subtracting its stress intensity factor from itself, using (3.7).

Therefore, the function $\tilde{u}_{2,0}^\delta$ has to satisfy the following problem

$$\begin{aligned} \mathcal{L}^0(\mathbf{x}, \nabla_{\mathbf{x}}) \tilde{u}_{2,0}^\delta &= - \sum_{\pm} \pi \mathcal{L}(S^\pm) \ell^\pm(u_{0,0}) \frac{(k_0/2)^{2\pi/\Theta}}{\Gamma(\pi/\Theta) \Gamma(\pi/\Theta + 1)} [\mathcal{L}^0(\mathbf{x}, \nabla_{\mathbf{x}}), \chi_\pm] \phi_2^\pm, & \text{in } \Omega \setminus \Gamma, \\ \mathcal{N}^0(\mathbf{x}, \nabla_{\mathbf{x}}) \tilde{u}_{2,0}^\delta &= 0, & \text{on } \partial\Omega, \\ (\mathcal{B}_\Gamma \tilde{u}_{2,0}^\delta)(\mathbf{x}) &= 0, & \text{on } \Gamma. \end{aligned} \quad (4.5)$$

The numerical effort to compute the corrector $\tilde{u}_{2,0}^\delta$ is the same as the numerical effort to compute the limit solution.

4.2. Computation of a reference solution and comparison

Computations are illustrated for the example 1.2. The meshes obtained for a thin plate perforated with 4 holes (Fig. 12a) and for a thin plate perforated with 8 holes (Fig. 12b) are refined close to the holes and resolve them.

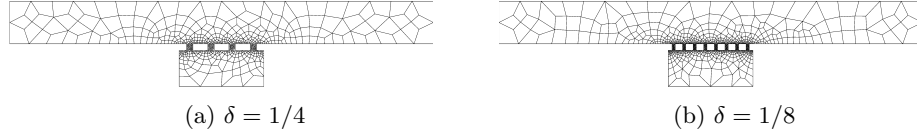


Fig. 12: Mesh used for the computation of the reference solution, for the porosity $\rho = 0.3$.

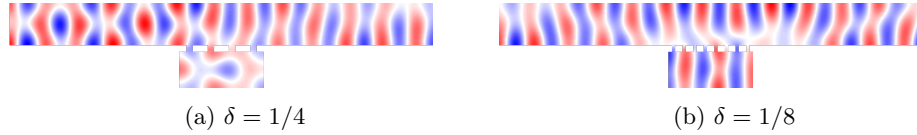


Fig. 13: Reference solution, for the porosity $\rho = 0.3$.

Study of the robustness of the error It was already studied in ¹² that the error estimate (1.4) holds for $(s, \kappa(s)) = (1, 0)$, $(s, \kappa(s)) = (\frac{4}{3}, 0)$ and $(s, \kappa(s)) = (2, 1)$, with a constant \mathfrak{C} depending on the canonical hole domain $\widehat{\Omega}_{\text{hole}}$. In particular, \mathfrak{C} depends on the porosity ρ of the thin plate. As it was already shown on Figures 7 and 9, this constant could possibly degenerate as $\rho \rightarrow 0$. To study, the robustness of the error, let $\delta = 1/8$ and let the height H of the canonical obstacle be obtained by parameter identification (*i. e.* $H = 0.6$).

On Figure 14, several plots of the L^2 macroscopic error (1.4) computed on the domain $\Omega_{0.25}$ are shown for different values of s : $(s, \kappa(s)) = (1, 0)$ corresponds to

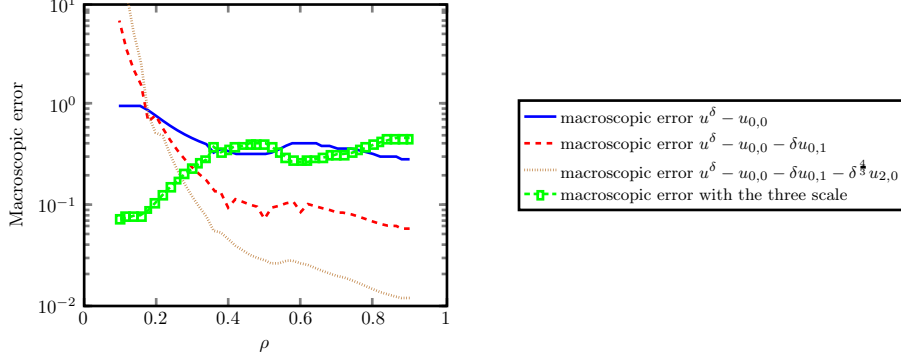


Fig. 14: Computation of the macroscopic error for the problem (P), taking into account more and more terms of the expansion, with respect to the porosity, and comparison with the macroscopic error obtained with a three scale strategy.

the macroscopic error between the reference solution u^δ and the limit macroscopic term $u_{0,0}$ (blue solid plot), $(s, \kappa(s)) = (\frac{4}{3}, 0)$ corresponds to the macroscopic error in which we take into account the first order corrector (red dashed plot), and $(s, \kappa(s)) = (2, 1)$ corresponds to the macroscopic error in which we take into account the second order corrector (brown dotted plot). For comparison, the plot of the L^2 macroscopic error (1.4) computed with s small and with a limit term obtained from a tree scale strategy (*i. e.* $\mathcal{B}_\Gamma v = ([v]_\Gamma - Z \langle \nabla v \cdot \mathbf{n} \rangle_\Gamma, [\nabla v \cdot \mathbf{n}]_\Gamma)^\top$) is shown using a green plot with squares. These different error curves show that, when the porosity ρ of the material is not too small, the application of this method with a two scale strategy gives a more and more accurate solution, when more and more macroscopic terms are considered in the expansion. *A contrario*, when the ρ is too small, the correctors degrade the obtained error, and it would be more appropriate to consider a three scale strategy.

Acknowledgment

The author would like to thank Robert Gruhlke (TU Berlin) for helpful discussions and partial implementation of the numerical experiments.

Appendix A. Appendix: definition of the profile function ψ_1^\pm

In this appendix, the construction of the angular function ψ_1^\pm that is used in the transmission conditions (3.3) and in the stress intensity factor (3.6) is detailed. Moreover, this function can be seen as the first element of a family of functions that can be derived by a general behavior of the form

$$\cos \frac{n\pi}{\Theta} (\theta^\pm - \Theta_0^\pm), \quad n \in \mathbb{N}^*.$$

This function is constructed as

$$\psi_1^\pm(\ln r^\pm, \theta^\pm) = \sum_{q=0}^2 \psi_{1,q}^\pm(\theta^\pm)(\ln r^\pm)^q, \quad w_{1,1,q,\pm} \in \mathcal{C}^\infty(\overline{I_1^\pm}) \cap \mathcal{C}^\infty(\overline{I_2^\pm}), \quad (\text{A.1})$$

where $I_1^\pm = (a^\pm, \gamma^\pm)$, $I_2^\pm = (\gamma^\pm, b^\pm)$ with $a^+ = 0, \gamma^+ = \pi, b^+ = \Theta$, and, $a^- = \pi - \Theta, \gamma^- = 0, b^- = \pi$. This function is constructed such that the function

$$v_1^\pm(r^\pm, \theta^\pm) := J_{\frac{\pi}{\Theta}-1}(k_0 r^\pm) \psi_1^\pm(\ln r^\pm, \theta^\pm)$$

satisfies

$$\left\{ \begin{array}{l} \Delta v_1^\pm + k_0^2 v_1^\pm = 0 \quad \text{in } \mathcal{K}_1^\pm \cap \mathcal{K}_2^\pm, \\ \partial_\theta v_1^\pm(r^\pm, a^\pm) = 0, \quad r^\pm > 0, \\ \partial_\theta v_1^\pm(r^\pm, b^\pm) = 0, \quad r^\pm > 0, \\ [v_1^\pm(r^\pm, \gamma^\pm)]_{\partial \mathcal{K}_1^\pm \cap \partial \mathcal{K}_2^\pm} = J_{\frac{\pi}{\Theta}-1}(k_0 r^\pm) \mathbf{a}_{1,1,\pm}, \quad r^\pm > 0, \\ [\partial_{\theta^\pm} v_1^\pm(r^\pm, \gamma^\pm)]_{\partial \mathcal{K}_1^\pm \cap \partial \mathcal{K}_2^\pm} = J_{\frac{\pi}{\Theta}-1}(k_0 r^\pm) \mathbf{b}_{1,1,\pm}, \quad r^\pm > 0, \end{array} \right. \quad (\text{A.2})$$

where

$$\mathcal{K}_j^\pm = \{(r^\pm \cos \theta^\pm, r^\pm \sin \theta^\pm) \in \mathcal{K}^\pm, r^\pm \in \mathbb{R}_+^*, \theta^\pm \in I_j^\pm\}, \quad j = \{1, 2\}, \quad (\text{A.3})$$

and,

$$\mathbf{a}_{1,1,\pm} = \mp \mathcal{D}_1^n \frac{\pi}{\Theta} \sin \frac{\pi^2}{\Theta}, \quad (\text{A.4})$$

$$\mathbf{b}_{1,1,\pm} = \mp \mathcal{N}_2^n \frac{\pi}{\Theta} \left(\frac{\pi}{\Theta} - 1 \right) \cos \frac{\pi^2}{\Theta} \pm \mathcal{N}_2^n \frac{\pi}{\Theta} \left(\frac{\pi}{\Theta} - 1 \right) \cos \frac{\pi^2}{\Theta}. \quad (\text{A.5})$$

In view of ¹², since $\lambda\Theta = \pi - \Theta$ is not a multiple of π , $\sin(\pi - \Theta) \neq 0$ the functions $\psi_{1,1}^\pm$ and $\psi_{1,2}^\pm$ are identically equal to 0. Therefore, ψ_1^\pm does not depend on $\ln r^\pm$, and there exists two constants $w_{1,+}^\pm$ and $w_{1,-}^\pm$ such that

$$\psi_1^\pm(\theta^\pm) = \begin{cases} w_{1,+}^\pm \cos\left(\frac{\pi}{\Theta} - 1\right) (\theta^\pm - \Theta_0^\pm), & \sin \theta^\pm > 0, \\ w_{1,-}^\pm \cos\left(\frac{\pi}{\Theta} - 1\right) (\theta^\pm - \Theta_0^\pm \mp \Theta), & \sin \theta^\pm < 0. \end{cases} \quad (\text{A.6})$$

We insert expression (A.6) in the Dirichlet and Neumann jump conditions, means the fourth and fifth lines of (A.2) gives, using that the jump is the limit value for $\theta^\pm > \gamma^\pm$ minus the limit value for $\theta^\pm < \gamma^\pm$ and using that $\gamma^\pm - \Theta_0^\pm = \pm\pi$:

$$\begin{aligned} w_{1,+}^\pm \cos\left(\frac{\pi}{\Theta} - 1\right) \pi - w_{1,-}^\pm \cos\left(\frac{\pi}{\Theta} - 1\right) (\pi - \Theta) &= \mp \mathbf{a}_{1,1,\pm}, \\ w_{1,+}^\pm \sin\left(\frac{\pi}{\Theta} - 1\right) \pi - w_{1,-}^\pm \sin\left(\frac{\pi}{\Theta} - 1\right) (\pi - \Theta) &= \frac{\mathbf{b}_{1,1,\pm}}{\left(\frac{\pi}{\Theta} - 1\right)}. \end{aligned} \quad (\text{A.7})$$

Determinant of system (A.7) is no other than $\sin(\pi - \Theta)$ which is non-zero by assumption on Θ . Therefore, this system is invertible, and we get

$$\begin{aligned} w_{1,+}^{\pm} &= \frac{1}{\sin(\Theta - \pi)} \left(\mp a_{1,1,\pm} \sin\left(\frac{\pi}{\Theta} - 1\right) (\pi - \Theta) + \frac{\Theta b_{1,1,\pm}}{\pi - \Theta} \cos\left(\frac{\pi}{\Theta} - 1\right) (\pi - \Theta) \right), \\ w_{1,-}^{\pm} &= \frac{1}{\sin(\Theta - \pi)} \left(\mp a_{1,1,\pm} \sin\left(\frac{\pi}{\Theta} - 1\right) \pi + \frac{\Theta b_{1,1,\pm}}{\pi - \Theta} \cos\left(\frac{\pi}{\Theta} - 1\right) \pi \right). \end{aligned} \tag{A.8}$$

References

1. A. Bensoussan, J. L. Lions, and G. Papanicolaou. *Asymptotic analysis for periodic structures Studies in Mathematics and its applications*, volume 5. North-Holland, Amsterdam, 1978.
2. A.-S. Bonnet-Ben Dhia, D. Drissi, and N. Gmati. Mathematical analysis of the acoustic diffraction by a muffler containing perforated ducts. *Math. Models Meth. Appl. Sci.*, 15(7):1059–1090, 2005.
3. H. Brezis. *Analyse fonctionnelle*. Collection Mathématiques Appliquées pour la Maîtrise. [Collection of Applied Mathematics for the Master’s Degree]. Masson, Paris, 1983. Théorie et applications. [Theory and applications].
4. D. Brown and D. Peterseim. A multiscale method for porous microstructures. *SIAM MMS*, 2016. Accepted for publication. Also available as INS Preprint No. 1410.
5. Stefan Busse-Gerstengarbe, Steffen Nitsch, Friedrich Bake, and Lars Enghardt. Study on a generic nonlocally reacting liner. *AIAA Journal*, 53(1):123–131, 2014.
6. X. Claeys and B. Delourme. High order asymptotics for wave propagation across thin periodic interfaces. *Asymptot. Anal.*, 83(1-2):35–82, 2013.
7. Concepts Development Team. *Webpage of Numerical C++ Library Concepts 2*. <http://www.concepts.math.ethz.ch>, 2016.
8. M. Dauge, S. Tordeux, and G. Vial. Selfsimilar perturbation near a corner: matching versus multiscale expansions for a model problem. In *Around the research of Vladimir Maz’ya. II*, volume 12 of *Int. Math. Ser. (N. Y.)*, pages 95–134. Springer-Verlag, New York, 2010.
9. B. Delourme, H. Haddar, and P. Joly. Approximate models for wave propagation across thin periodic interfaces. *J. Math. Pures Appl. (9)*, 98(1):28–71, 2012.
10. B. Delourme, K. Schmidt, and A. Semin. When a thin periodic layer meets corners: asymptotic analysis of a singular Poisson problem. Technical report, 2015.
11. B. Delourme, K. Schmidt, and A. Semin. On the homogenization of thin perforated walls of finite length. *Asymptotic Analysis*, 97(3-4):211–264, 2016.
12. B. Delourme, K. Schmidt, and A. Semin. On the homogenization of the Helmholtz problem with thin perforated walls of finite length. submitted for publication.
13. Theo Fett. *Stress Intensity Factors, T-stresses, Weight Functions: Supplement Volume*, volume 55. KIT Scientific Publishing, 2009.
14. Ph. Frauenfelder and Ch. Lage. Concepts – an object-oriented software package for partial differential equations. *ESAIM: Math. Model. Numer. Anal.*, 36(5):937–951, 2002.
15. Christina Frederick and Bjorn Engquist. Numerical methods for multiscale inverse problems. *ArXiv e-prints*, 2014.
16. Christophe Geuzaine and Jean-François Remacle. Gmsh: A 3-d finite element mesh generator with built-in pre-and post-processing facilities. *International Journal for Numerical Methods in Engineering*, 79(11):1309–1331, 2009.

17. D. Gómez Pedreira and P. Joly. A method for computing guided waves in integrated optics. Part II: Numerical approximation and error analysis. *SIAM J. Numer. Anal.*, 39(5):1684–1711, 2002.
18. H. Haddar, P. Joly, and H.M. Nguyen. Generalized impedance boundary conditions for scattering by strongly absorbing obstacles: the scalar case. *Math. Models Methods Appl. Sci.*, 15(8):1273–1300, 2005.
19. David P Hewett and Ian J Hewitt. Homogenized boundary conditions and resonance effects in faraday cages. In *Proc. R. Soc. A*, volume 472, page 20160062. The Royal Society, 2016.
20. Patrick Joly and Adrien Semin. Construction and analysis of improved kirchoff conditions for acoustic wave propagation in a junction of thin slots. *ESAIM: proceedings*, 25:44–67, 12 2008.
21. Patrick Joly and Adrien Semin. Propagation of an acoustic wave in a junction of two thin slots. Technical report, INRIA Research Report, 10 2008.
22. V. A. Kondrat'ev. Boundary-value problems for elliptic equations in conical regions. *Dokl. Akad. Nauk SSSR*, 153:27–29, 1963.
23. C. Lahiri, S. Sadig, M. Gerendas, L. Enghardt, and F. Bake. Establishment of a high quality database for the modelling of perforated liners. *J. Eng. Gas Turbines Power*, 133(9):091503–1–091503–9, 2011.
24. S. Laurens, S. Tordeux, A. Bendali, M. Fares, and P.R. Kotiuga. Lower and upper bounds for the Rayleigh conductivity of a perforated plate. *ESAIM: Math. Model. Numer. Anal.*, 47:1691–1712, 11 2013.
25. Sophie Laurens, Sébastien Tordeux, Abderrahmane Bendali, M'Barek Fares, and P. Robert Kotiuga. Lower and upper bounds for the Rayleigh conductivity of a perforated plate. *ESAIM: Mathematical Modelling and Numerical Analysis*, 47(6):1691–1712, November 2013.
26. V. Maz'ya, S. Nazarov, and B. Plamenevskij. *Asymptotic theory of elliptic boundary value problems in singularly perturbed domains. Vol. I*, volume 111 of *Operator Theory: Advances and Applications*. Birkhäuser Verlag, Basel, 2000. Translated from the German by Georg Heinig and Christian Posthoff.
27. S. A. Nazarov. Asymptotic behavior of the solution of the Dirichlet problem in an angular domain with a periodically changing boundary. *Mat. Zametki*, 49(5):86–96, 159, 1991.
28. S. A. Nazarov. Asymptotic behavior of the solution and the modeling of the Dirichlet problem in an angular domain with a rapidly oscillating boundary. *Algebra i Analiz*, 19(2):183–225, 2007.
29. S. A. Nazarov. The Neumann problem in angular domains with periodic and parabolic perturbations of the boundary. *Tr. Mosk. Mat. Obs.*, 69:182–241, 2008.
30. J. Sanchez-Hubert and E. Sanchez-Palencia. Acoustic fluid flow through holes and permeability of perforated walls. *J. Math. Anal. Appl.*, 87(2):427 – 453, 1982.
31. Anita Schulz, Daniel Haufe, Jürgen Czarske, Andreas Fischer, Friedrich Bake, and Lars Enghardt. Spectral analysis of velocity fluctuations in the vicinity of a bias flow liner with respect to the damping efficiency. *Acta Acustica united with Acustica*, 101(1):24–36, 2015.
32. Christoph Schwab. *p- and hp-finite element methods: Theory and applications in solid and fluid mechanics*. Oxford University Press, Oxford, UK, 1998.